

## V. EXPERIMENTAL DESIGN ISSUES

### V.A. LANSCE Pulsed Cold Neutron Beam

The UCN production rate in the superthermal LHe source depends upon the neutron beam spectral density  $d^2\Phi/d\lambda d\Omega$  at 8.9 Å, as is discussed in chapter V.B. Neutrons with a different wavelength than 8.9 Å will not downscatter to make UCNs but instead will pass through the apparatus or will be scattered and absorbed by surrounding materials. Some of betas and gamma rays from the decay processes can then interact with the liquid helium in the measurement cells, producing scintillation light that affects the signal-noise ratio of the EDM measurement. To reach its goal, the EDM experiment requires the maximum flux of 8.9-Å neutrons from the source and beamline. The monochromatism,  $\Delta\lambda/\lambda$ , of the 8.9 Å beam should be  $\sim 1\%$ . The beam should be highly polarized with a minimum of fast neutrons or high-energy gamma-rays. Its phase space should match the UCN production cells.

#### V.A.1. Cold Moderator of the LANSCE Spallation Source

At the LANSCE spallation neutron source, 800-MeV proton pulses, at the rate of 20 Hz, interact with the tungsten target producing fast neutrons that are partially moderated by a super-cooled hydrogen gas moderator. The EDM experiment will be mounted behind the  $n+p \rightarrow d+\gamma$  experiment on a new cold neutron beamline, flight path 12, at the Lujan Center. This beamline views the new upper tier cold hydrogen moderator. The calculated performance of this coupled moderator, including the time and energy spectra of a neutron pulse, are described in Ref. [1]. Figure V.A.1. shows the calculated average moderator brightness as a function of the neutron energy (the energy of the 8.9 Å neutron is about 1 meV) for hydrogen with an ortho-para ratio of 1. The brightness is obtained from the MCNPX moderator model calculations [1,2] that have been scaled according to experimental results from the flight path 11A cold moderator [3].

#### V.A.2. Beamline of the EDM experiment

The beamline for the EDM experiment will be built as an extension from the  $n+p \rightarrow d+\gamma$  experiment on the flight path 12. The beamline of the  $n+p \rightarrow d+\gamma$  experiment that is under construction is shown in figure V.A.2. The neutron guide of the  $n+p \rightarrow d+\gamma$  beamline ends 21 m from the moderator. For the EDM experiment, a section of neutron guide will be installed through the  $n+p \rightarrow d+\gamma$  cave. At the end of the cave, a Bi filter will be mounted, and it will be followed by a  $t_0$  chopper located in place of the  $n+p \rightarrow d+\gamma$  beam stop.

Downstream of the chopper, the 8.9-Å neutrons will be split to two beams, polarized in opposite directions, and guided to the measurement cells that are located at 31 m from the moderator. The floor plan of the EDM beamline and the experiment is shown in figure V.A.3.

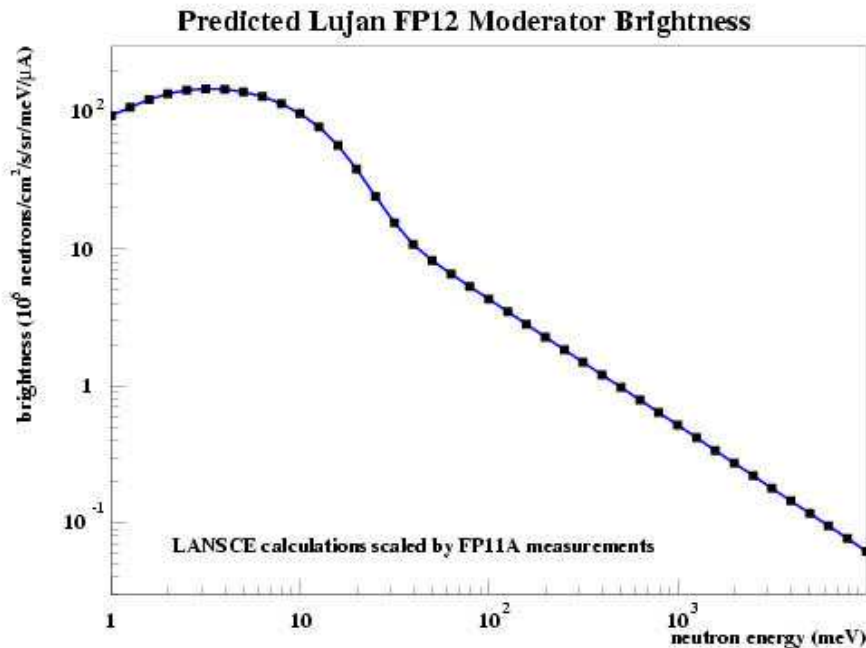


Fig. V.A.1. Calculated average brightness of the coupled-hydrogen moderator, with an ortho-para ratio of 1, viewed by flight path 12.

### V.A.3. Cold Neutron Beam Line

The  $n+p \rightarrow d+\gamma$  beamline has three main components inside LANSCE experimental room 1 (ER1). The first is a 4-m long neutron guide that is placed inside the biological shield and that starts at about 1.3 m from the moderator surface. The second is an external, 2-m long guillotine-type shutter system that contains a neutron guide and is placed next to the biological shield. And the third is a two-blade frame-definition chopper that is located at 9.3 m from the moderator. The heavy integrated radiological shielding that contains all the ER1 beamline components is not shown in figure V.A.2. After the chopper, a guide that ends at 21 m from the moderator transports the neutrons to the  $n+p \rightarrow d+\gamma$  cave. The straight supermirror coated guide has the inner cross section of 9.5 cm  $\times$  9.5 cm and the relative reflectivity of  $m = 3$  ( $m = 1$  is the reflectivity of  $^{58}\text{Ni}$  coated guide). The glass neutron guide is held in a steel vacuum tube. There is considerable uncertainty in the brightness given in Figure V.A.1, and we prefer to use the flux plotted in Figure V.A.4 as

a function of time-of-flight (TOF) on Flight Path 12, 24.3 m from the source. The neutron transport calculations were scaled from measurements on Flight Path 11 assuming an average proton current of  $150 \mu\text{A}$ . The arrow indicates the TOF of 54.5 ms for  $8.9\text{-}\text{\AA}$  neutrons at 24.3 m. The flux of  $8.9\text{-}\text{\AA}$  neutrons is  $1 \times 10^5 \text{ neutrons/ms/pulse/cm}^2 = 5.4 \times 10^7 \text{ neutrons/meV/cm}^2/\text{s} = 1.2 \times 10^7 \text{ neutrons/\AA/cm}^2/\text{s}$ .

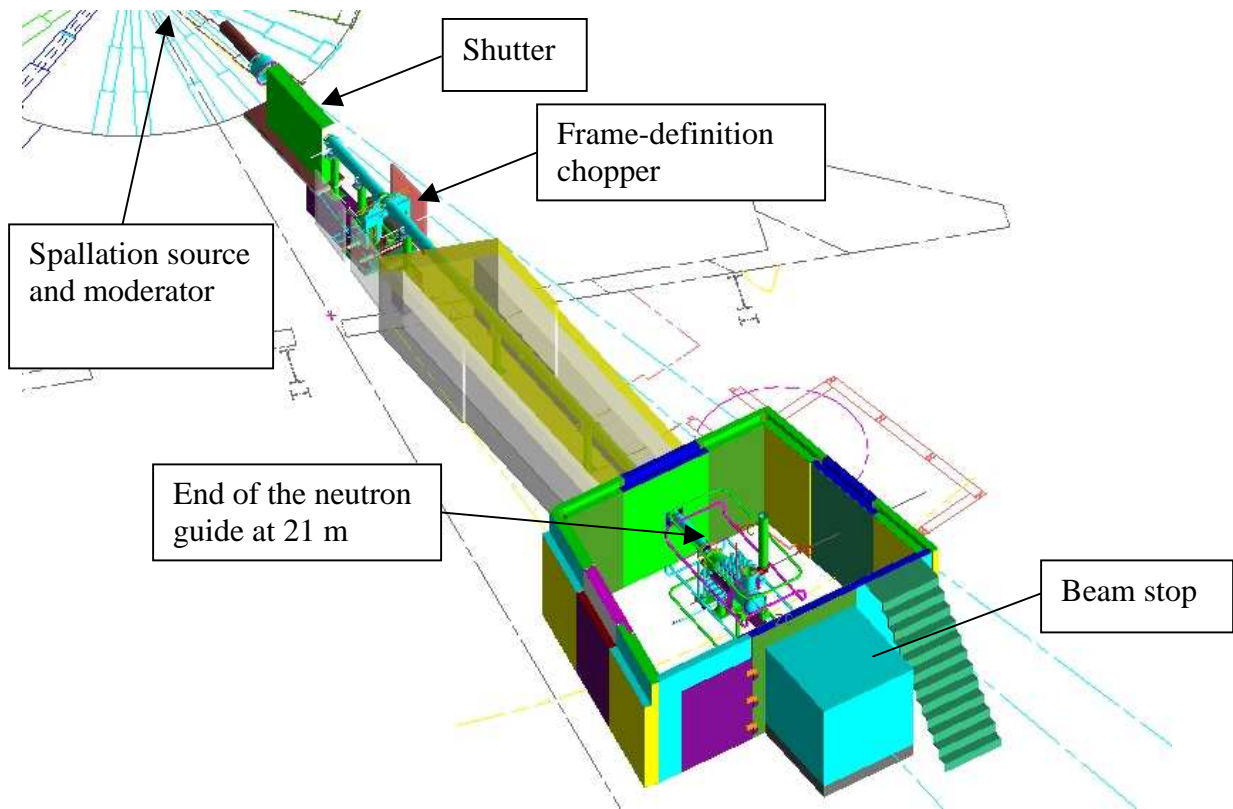


Figure V.A.2 A 3D-model view of the  $n+p \rightarrow d+\gamma$  beamline at the Lujan Center.

#### V.A.4. Frame-Definition Chopper

An advantage of a spallation neutron source is that TOF can be used to select the neutron energy. At low neutron energies a frame-definition chopper is used to select the TOF window of interest. Figure V.A.5. shows an evolution of the flight of the  $8.9 \text{ \AA}$  neutrons from the source to the EDM experiment in three 50-ms wide frame. A two-blade frame definition chopper (FDC) is located at 9.38 m from the moderator. For a 45-cm radius aluminum chopper blade rotating at 20 Hz, it takes 1.88 ms to sweep across the  $9.5 \text{ cm} \times 9.5 \text{ cm}$  guide. If the phase of FDC blade is selected so that the guide is fully open when the  $8.9\text{\AA}$  neutrons have reached the chopper, the 3.76-ms chopper opening corresponds

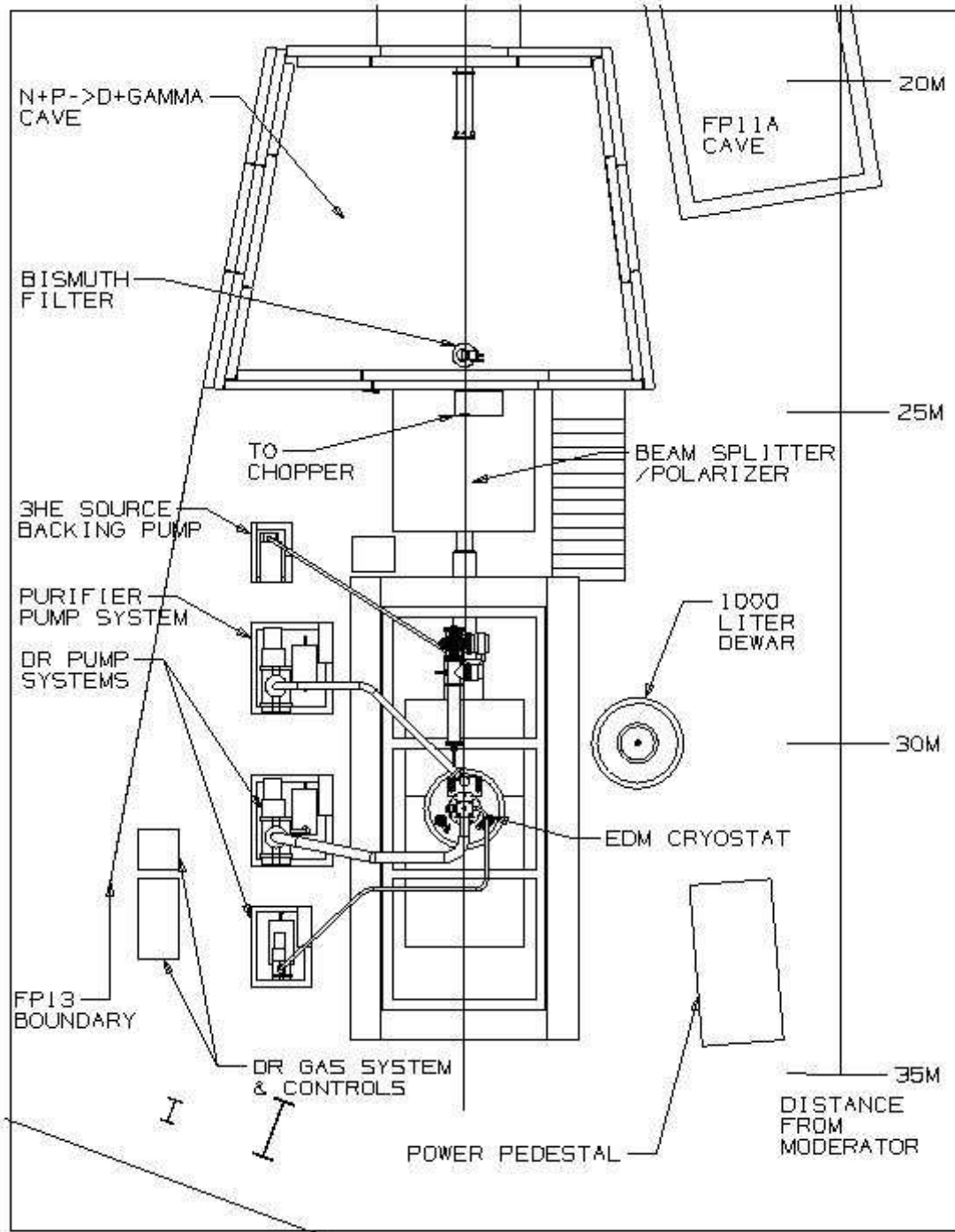


Fig. V.A.3. Floor plan of the EDM experiment on flight path 12 at the Lujan Center.

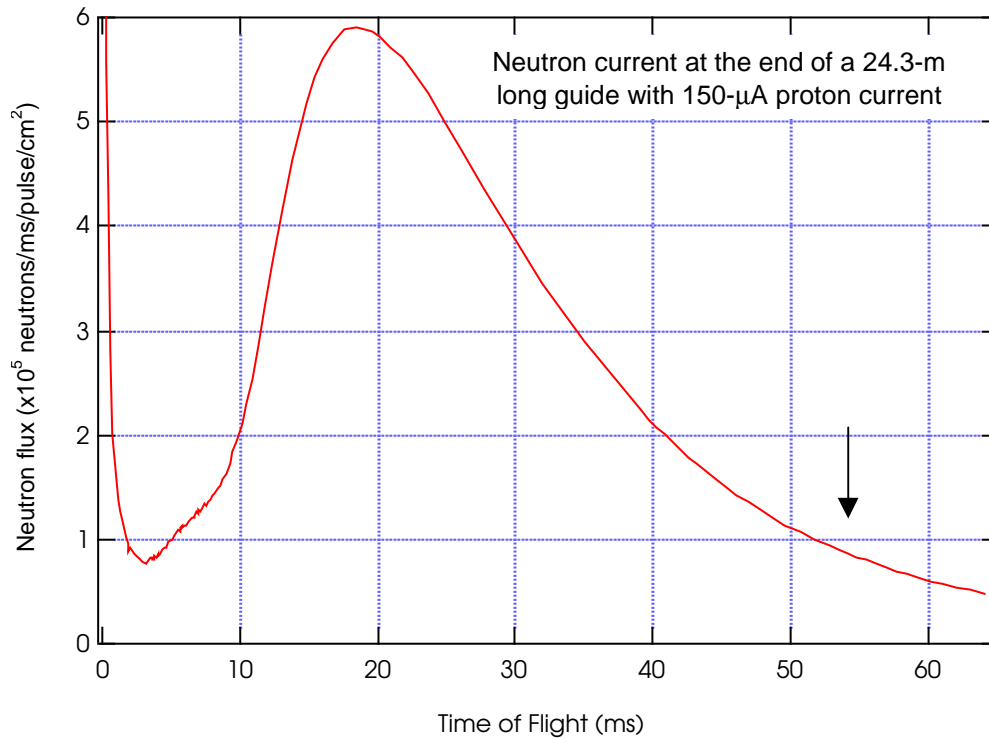


Fig. V.A.4. Neutron flux plotted as a function of TOF at the end of the neutron guide of Flight Path 12, 24.3 m from the moderator. The next proton pulse comes at 50 ms. The arrow indicates a TOF of 54.5 ms corresponding to 8.9-Å neutrons at 24.3m and corresponds to a flux of  $5.4 \times 10^7$  neutrons/meV/cm<sup>2</sup>/s.

to neutron energies from 0.88 to 1.25 meV. When the chopper is closed, the neutrons will be absorbed by a 0.01 inch thick Gd coating on the aluminum plate. This thickness of Gd is sufficient to allow only 0.1% of 100-meV neutrons to be transmitted. At lower neutron energies the neutron-Gd capture cross section increases as  $1/v$ , where  $v$  is the neutron velocity. The brown bands in figure V.A.5. represent the TOF of the fast neutrons down to 100 meV. Most of these neutrons will not be absorbed by the Gd coating and have to be removed from the beam in another way. Figure V.A.5 also indicates the locations of the  $n+p \rightarrow d+\gamma$  cave, the Bi filter, the  $t_0$  chopper in the  $n+p \rightarrow d+\gamma$  beam stop, and the EDM experiment.

### V.A.5 Bismuth Filter for Fast Neutrons

A polycrystalline Bragg scattering filter will remove most of the fast neutrons and gamma rays from a neutron beam. The Bragg filter becomes transparent at wavelengths greater than  $2d$ , where  $d$  is the lattice parameter of the filtering material. The cut-off wavelength of Bi is about 6.8 Å. The cut-off is sharp if the filter is cooled to low

temperatures. A filter length of 20 cm transmits only neutrons with energies less than 1.7 meV (6.8 Å). Figure V.A.6. shows the 20-cm long Bragg-scattering bismuth filter constructed for use in the experiment. The Bi block is cooled with a cryo-cooler to 14 K. This filter system was tested during the 2001-test run in the flight path 11A, and the results obtained relative to transmission data are presented in figure V.A.7. The data are neutron counts measured by a  ${}^6\text{Li}$ -glass scintillator. The long wavelength neutron spectrum was measured through a 0.031-inch diameter hole in a Cd sheet. The fast neutron transmission through the Bi filter was obtained by using a piece of a  ${}^6\text{Li}$ -loaded plastic sheet in the front of the hole to remove the low energy neutrons. The absorber was especially effective on the neutrons from the previous frame, which arrived after the second proton pulse, at the detector positioned at 23 m. From these transmission measurements we can conclude that the transmittance of the short wavelength neutrons through the Bi filter is about 2% and that the filter has no significant effect on the 8.9 Å neutron flux.

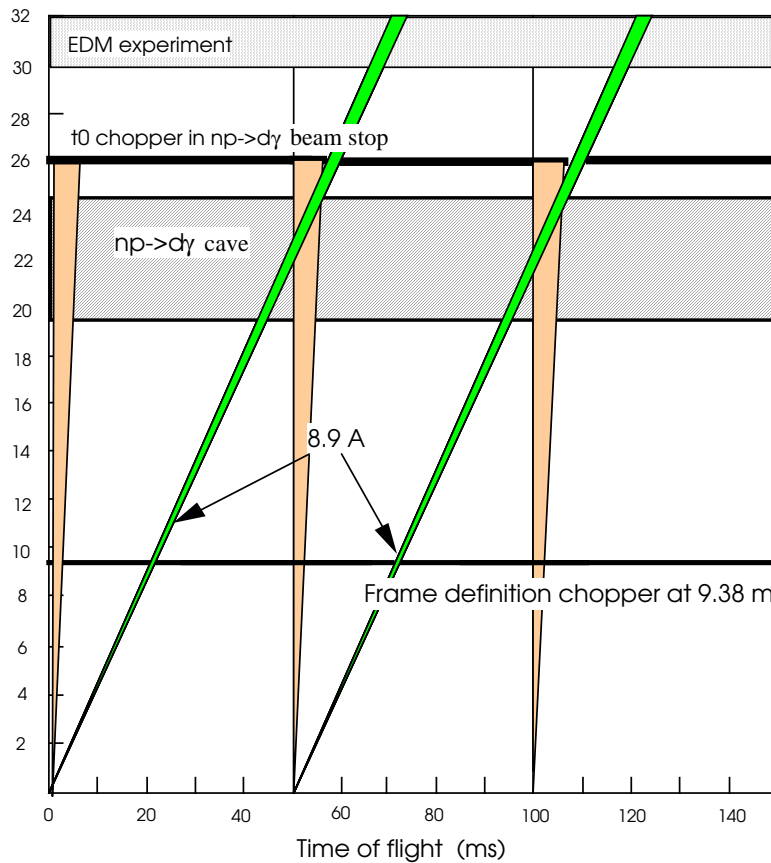


Fig. V.A.5. Timing diagram of the 8.9-Å neutrons from the source to the EDM experiment.

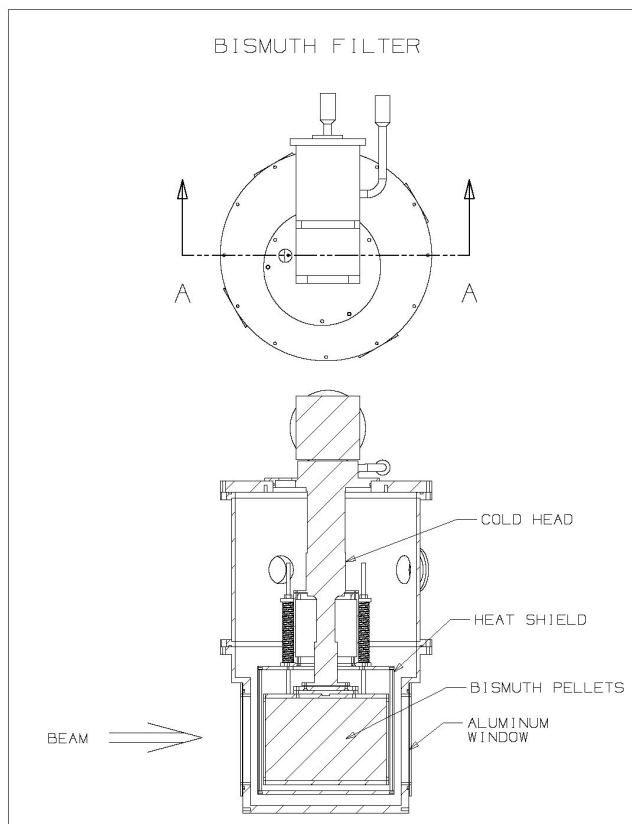


Fig. V.A.6 The cryogenic Bragg scattering Bismuth filter.

### V.A.6. Fast Neutron and Gamma Ray Backgrounds

A proton pulse interacting with the tungsten target in the spallation source creates a high-intensity gamma ray and fast neutron burst that decays in a few milliseconds. In addition to the gamma rays and fast neutrons, activated beam line components create an additional small constant gamma ray background. The fast neutrons and gamma rays in the beam can be removed without affecting the flux of the long wavelength neutrons of interest with a  $t_0$  chopper. The rotor of a typical Lujan  $t_0$ -chopper is made from 30-cm thick heavy material like Inconel or tungsten. To minimize the opening and closing times of the chopper, they normally run at two or three times the repetition rate of the neutron source. With the  $t_0$ -chopper located in the  $n+p \rightarrow d+\gamma$  beam stop, there is about 2 ms separation between the 8.9-Å neutrons and the tail of the fast neutron pulse, and therefore the high rotational rate of the chopper will need to be reserved.

The total neutron cross section on Inconel alloy (Ni-Fe-Cr-Ti) in the eV-keV energy range is about 7 barns, giving an effective transmission through a 30-cm thick Inconel rotor of about  $1 \times 10^{-8}$ . For 2-MeV photons the transmission factor is  $3 \times 10^{-6}$ .

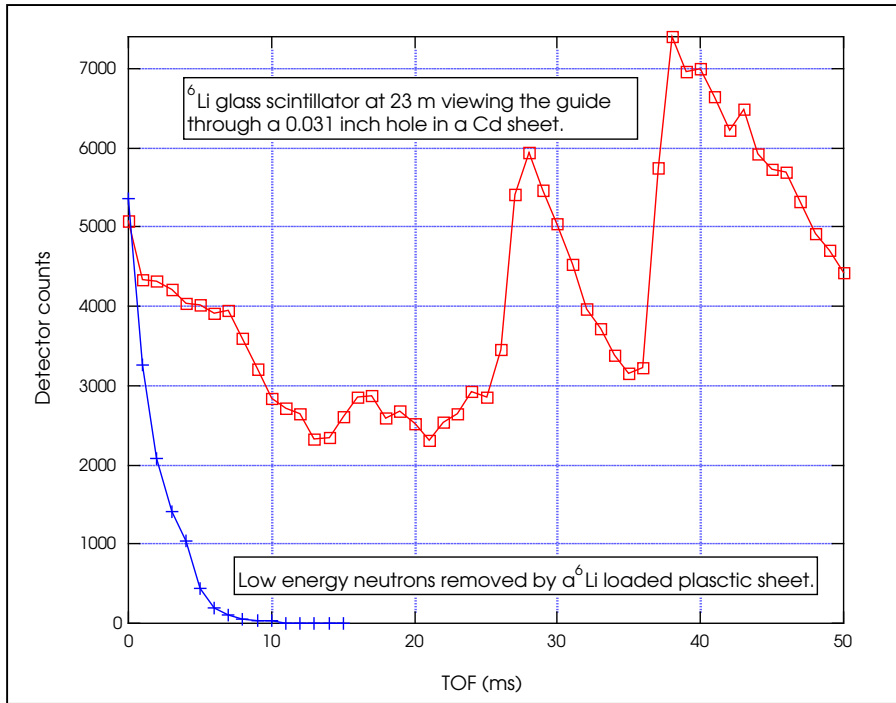


Fig. V.A.7. Relative transmission of the 20-cm long cold Bi filter as a function of TOF. The transmission of the fast neutrons is also shown when a sheet of  $^6\text{Li}$ -loaded plastic was used to remove the long-wavelength neutrons.

In addition to the  $t_0$  chopper attenuation, the Bi filter also significantly attenuates fast neutrons and gamma rays. If the effective thickness of the Bi filter is 15 cm, then the transmission fraction for the photons is about  $6 \times 10^{-4}$ . The thickness of the  $t_0$  chopper will be reevaluated with MCNPX calculations to account for the effect of the Bi filter.

Both the Bi filter and the  $t_0$  chopper are proposed because the Bi filter always attenuates the high-energy particles, regardless of its temperature. This fail-safe behavior permits the use of lower cost shielding downstream of the chopper, especially for the cover of the EDM cryostat.

### V.A.7. Neutron Spin State Selector and Spin Rotator

The reference design of the EDM apparatus has two measurement cells in order to cancel systematic errors. To effectively fill the cells, the neutron beam must be split in two. The optimization of the available floor space behind the  $n+p \rightarrow d+\gamma$  beam stop requires that the  $t_0$  chopper be placed inside the beam stop. Then in roughly four meters between the chopper and the cryostat, the neutron beam must be divided. Additionally, if these two beams are polarized, the sensitivity of the experiment to the polarization of the  ${}^3\text{He}$  is significantly reduced because the  ${}^3\text{He}$  will not be needed to polarize the neutrons. The design concept of the polarizing neutron beam splitter guide is shown in Fig. V.A.8. This concept is an adaptation of the splitter used at the Hahn-Meitner Institute [4].

In the ferromagnetic medium the refractive index has two-values

$$n^\pm \cong 1 - \frac{\lambda^2}{2\pi} N(a_n \mp a_m),$$

where  $\lambda$  is the wave length of the neutrons,  $N$  is the density,  $a_n$  is the nuclear scattering length, and  $a_m$  is the magnetic scattering length given by

$$a_m = \frac{m_n \mu_n}{2\pi \hbar^3} \int B d^3 r.$$

Here  $m_n$  is the neutron mass,  $\mu_n$  the neutron magnetic moment, and  $B$  is the magnetic field in the magnetized ferromagnetic material. The integral is over the volume of lattice occupied by the ferromagnetic atom. The polarizing neutron beam splitter is formed by two total reflecting magnetic supermirror surfaces set at the angle of  $\pm\theta_c/2 = 1.6^\circ$ . The magnetic supermirror elements are fabricated by alternating layers of a FeCo alloy and Si deposited on Si wafers that have a high neutron transmission. The application of a 300-gauss magnetic field will change the critical angle of the reflection depending on the direction of the neutron spin. The critical angle of one spin state will be increased by the magnetic scattering length and the supermirror surface will reflect the neutron up to the critical angle and transmit the other spin state. Hence, a neutron with one spin state is reflected into one of the deflected guides while the opposite spin state is reflected into the second guide. The outgoing guides are set to  $\pm\theta_c = 3.2^\circ$ . The guides will be turned parallel just before entering the cryostat. Before the cryostat, adiabatic spin-rotating RF coils will be mounted to allow a manipulation of the neutron-spin direction.

A rudimentary Monte-Carlo simulation has been used to evaluate the performance of the polarizing neutron beam splitter. The simulation assumes perfect reflection from supermirror walls and perfect performance of the magnetic supermirrors. The result is that there is a total transmission of 45% of the incident beam down each channel, i.e. half

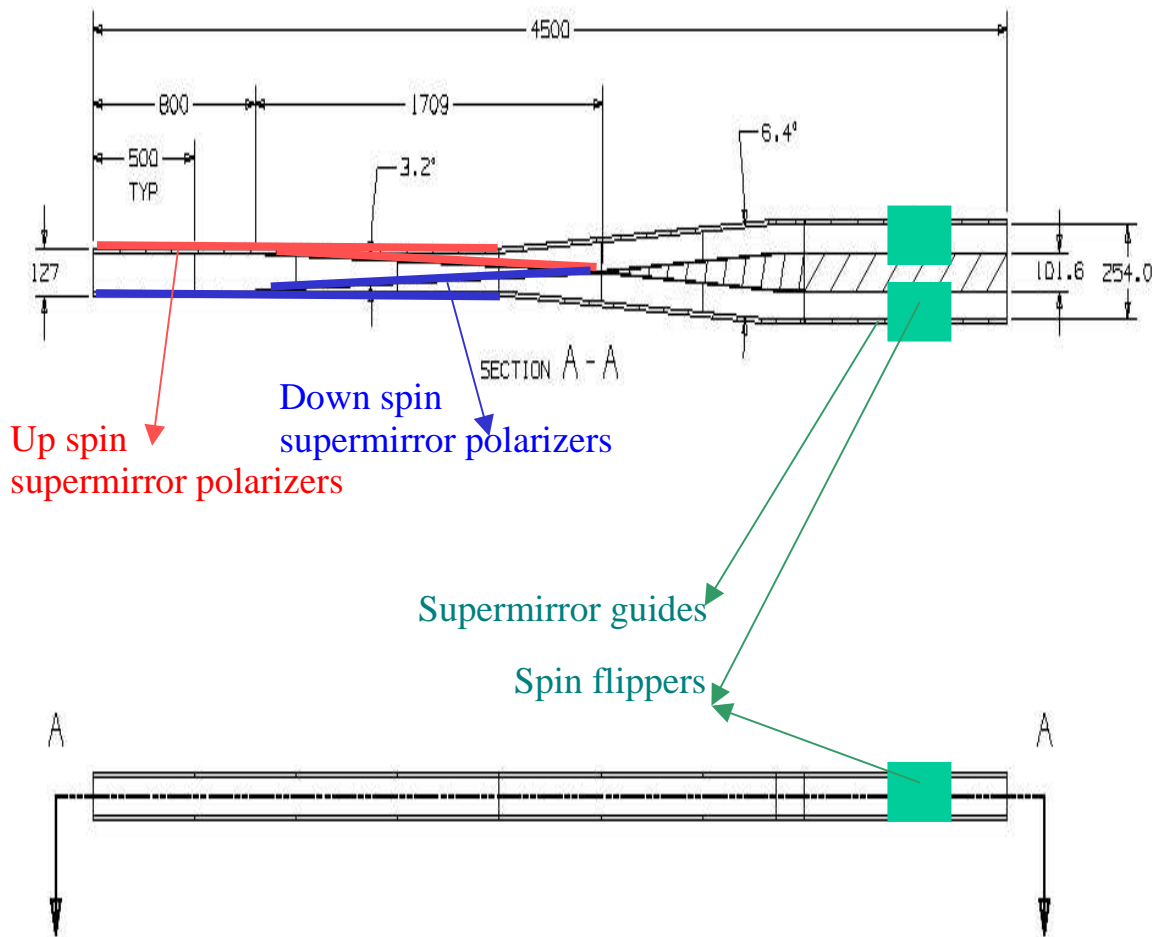


Fig. V.A.8. Polarizing neutron beam splitter, dimensions are in mm. The scales in the two dimensions are not the same.

of the total beam is lost. The losses are because the critical angle needs to be  $\pm\theta_c/4$  for high transmission and polarization. There is insufficient space between the  $t_0$  chopper and the cryostat to accommodate the proper length of the splitter guide that should be  $\sim 14$  m. Many neutrons incident the walls with an angle greater than  $\pm\theta_c$  after reflections. Additionally, polarization of the beams is only 16%. This low polarization is due to a nearly equal superposition of trajectories with an angle greater than  $\pm\theta_c/2$  with trajectories with an angle less than  $\pm\theta_c/2$ . The polarization can be recovered at the cost of neutron flux by placing magnetic supermirrors, backed with a neutron absorbing material,

along the incoming guide with their magnetization as shown in the Fig. V.A.8. With the length adjusted to remove only large-angle events, the simulation predicts that the transmission of the channels will be reduced to 24% of that possible, but the polarization will be 99%. The polarization sensitive lining effectively reduces the phase space. More modeling is required to optimize the beam splitter parameters for the needs of the experiment.

The splitter losses depend strongly on the assumption that the phase space is uniformly filled with neutrons up to  $\pm\theta_c$ . The losses in the guide, taken into account in Fig. V.A.4 are essentially all the large angle neutrons, and the splitter performance can be expected to be much better than calculated. In fact, the polarization absorbers on the walls may not be needed.

During the evaluation of the splitter, an arrangement was investigated where all the angles were set to  $\pm\theta_c/4$ . This splitter has a transmission of 63% down each channel and a polarization of 99%. Unfortunately, the length of the splitter is 14 m and cannot fit to the available footprint in the LUJAN experimental room 2. However, there is an ample room to match the ballistic transport of the proposed SNS beam line. The tiles of magnetic supermirrors from the flight path 12 arrangement at LANSCE can be reused in the SNS setup. The factor of 2.5 in the intensity from the SNS splitter is an additional gain over the relative neutron flux from the SNS spallation sources.

#### **V.A.8. Neutron Beam in the Cryostat**

The neutron beam will enter the cryostat through Be windows. Beryllium was selected because it has no long-lived isotopes made in neutron capture reactions. It also does not become superconducting at low operating temperatures of the cryostat. The distance between the cryostat entry window and the measuring cells is about one meter. Due to the phase space, half of the neutrons would not enter the measuring cells. To keep the neutrons, supermirror guide sections will be installed into the cryostat, one for each measuring cell. Gradual cooling will be necessary in order not to damage these guides, and they must stop far enough in front of the cells so that the dielectric will not distort the electric field.

#### **V.A.9. Radiological Shielding of the EDM apparatus**

Because of the long flight path (a small solid angle), the frame-definition chopper, the  $t_0$  chopper, and the Bi filter, only 8.9 Å neutrons can reach the EDM experiment. The short

wavelength neutrons are scattered by the  $t_0$  chopper and the Bi filter, and finally blocked by the beam splitter. After the  $t_0$  chopper additional gamma rays are created in the splitter where half of the neutron beam will be absorbed. This section of the beamline requires a thicker shielding that must be evaluated along with the rest of the neutron shielding around the experiment.

#### **V.A.10. Flux of the 8.9 Å Neutrons to the UCN Production Cells**

We can estimate the flux of 8.9-Å neutrons in the UCN production cell. At the end of the guide at 24 m the flux is  $5.4 \times 10^7$  neutrons/meV/cm<sup>2</sup>/s. Due to the phase space of the beam, there will be losses in the Bi filter and the  $t_0$  chopper. The total length of the section without guide is about 50 cm long and will transmit 80% of the neutrons. The transmission of the polarizing beam splitter is quite uncertain as noted above. Due to the uncertainties, we use unit transmission in this region for our calculations, and future results can be scaled later.

#### **References**

- [1] Phillip D. Ferguson, Gary J. Russell, and Eric J. Pitcher, "Reference Moderator Calculated Performance For The LANSCE Upgrade Project," *ICANS-XVIII: Proceedings of the Thirteenth Meeting of the International Collaboration on Advanced Neutron Sources*, Paul Scherrer Institut report PSI Proceedings 95-20, ISSN 1019-6447, pp. 510-517 (November 1995).
- [2] G. J. Russell, P. D. Ferguson, and E. J. Pitcher, "The Lujan Center: A Pulsed Spallation Neutron Source At Los Alamos," in *the Proceedings of ICON-8: the Eighth International Conference on Nuclear Engineering*, April 2-6, 2000, Baltimore, Maryland, pp.1-12.
- [3] G. Mitchell *et al.*, The LANSCE flight path 11A moderator brightness. Private communication.
- [4] Th. Krist, C. Pappas, Th. Keller, and F. Mezei, *Physica* **B213&214** 939 (1995).